Fusion Engineering and Design 222 (2026) 115508

Contents lists available at ScienceDirect

Fusion Engineering and Design

journal homepage: www.elsevier.com/locate/fusengdes

Fluid-dynamic and thermo-mechanical analyses of the metallic steering mirror for the ECRH system of DTT

Alfredo Pagliaro [a,*], Avelino Mas Sánchez [b], Francesco Braghin [a], Alessandro Bruschi [c], Daniele Busi [a], Francesco Fanale [c], Gustavo Granucci [c,e], Cinta Marraco Borderas [b], Afra Romano [d,e], Anastasia Xydou [b], Fabio Zanon [f]

[a] Politecnico di Milano, Department of Mechanical Engineering, Via Giuseppe La Masa 1, Milano, 20156, Italy
[b] Ecole Polytechnique Fédérale de Lausanne (EPFL), Swiss Plasma Center (SPC), CH-1015 Lausanne, Switzerland
[c] Institute for Plasma Science and Technology – National Research Council of Italy, Via Roberto Cozzi 53, Milano, 20125, Italy
[d] ENEA, Technology for Nuclear Safety and Security Department, Via Enrico Fermi 45, Frascati, 00044, Roma, Italy
[e] DTT S.C. a r.l, Via E. Fermi 45, Frascati, 00044, Roma, Italy
[f] Eni S.p.A., Piazzale Enrico Mattei 1, 00044, Roma, Italy

ARTICLE INFO

Keywords:
Heat sink
Microwave technology
Steering mirror
Metallic material
Electromagnetic forces
CFD
FSI
ECRH

ABSTRACT

The steerable launcher mirrors accurately guide microwave beams into the plasma, which is a fundamental function within the Electron Cyclotron Resonance Heating (ECRH) system of the Divertor Tokamak Test (DTT) facility, currently being built in Frascati, Italy. Since the mirror is subjected to intense electromagnetic field variations, which could induce high loads leading to structural failure, it is essential to identify a trade-off between thermomechanical performance and an adequate material selection with lower electrical conductivity which limits the electromagnetic induced loads. This paper investigates the two main configurations of metallic mirrors: monolithic Inconel 718 and a bimetallic design combining Stainless Steel 316 L and CuCrZr. The study covers thermo-fluid dynamic and thermomechanical analyses to assess the mirror's resistance under the imposed heat flux conditions. Furthermore, a fatigue analysis is conducted to evaluate the component's life cycle. Finally, different configurations are compared, highlighting how the two main proposed solutions offer the best compromise between electromagnetic forces and thermomechanical stresses.

1. Introduction

The Divertor Tokamak Test (DTT) facility [1], currently under construction in Frascati, Italy, is intended to explore a range of divertor configurations under plasma conditions representative of those expected in DEMO. To ensure the relevance of these investigations for next-generation fusion reactors, the divertors in DTT will be subjected to high heat fluxes coming from plasma operation. This requires a robust Heating and Current Drive system, incorporating multiple techniques such as Neutral Beam Injection (NBI), Ion Cyclotron Resonance Heating (ICRH), and Electron Cyclotron Resonance Heating (ECRH) [2]. The ECRH system, in particular, is designed to deliver the power of 32 gyrotrons, each rated at 1 MW, operating at a frequency of 170 GHz with pulse durations of up to 100 s [3]. Gyrotrons are grouped into four clusters of eight units each, with the generated microwave power transmitted via quasi-optical, evacuated multibeam transmission lines to the tokamak [4]. The system employs 32 front-steering launchers distributed across four sectors of the machine, with each sector housing six equatorial and two upper launchers [5]. As shown in Fig. 1. each launcher includes a fixed focusing mirror (M1) and a planar, steerable mirror (M2) [6].The latter can be controlled individually for power deposition in plasma at different locations. During reflection, ohmic losses in conductive components induce substantial thermal loads on the mirror surfaces. These loads are further intensified by plasma radiation and nuclear heating. Given the long plasma pulse durations, an active water-cooling system is required to control mirror temperatures and limit structural deformation [7,8]. Due to the high thermal and electromagnetic loads, a thorough investigation of the selected materials is

* Corresponding author.
E-mail address: alfredo.pagliaro@polimi.it (A. Pagliaro).

https://doi.org/10.1016/j.fusengdes.2025.115508
Received 10 September 2025; Received in revised form 15 October 2025; Accepted 28 October 2025

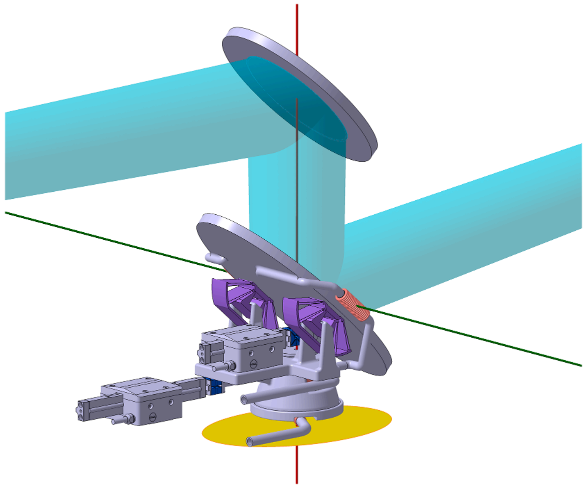

Fig. 1. Setup of the M1 and M2 mirrors for the ECRH system of DTT.

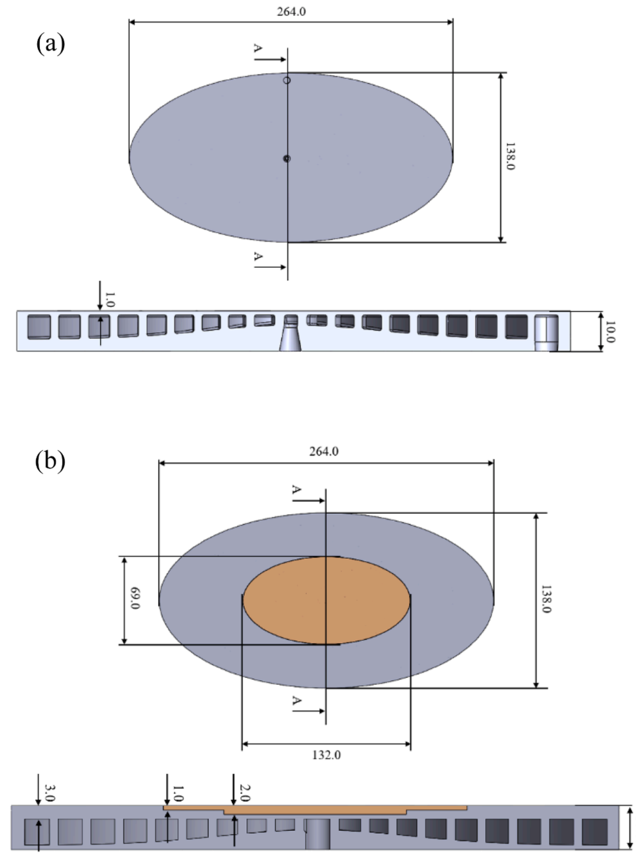

Fig. 2. (a) Launcher mirror assembly in monolithic Inconel 718. (b) Bimetallic launcher mirror configuration: SS316L bulk with a CuCrZr surface layer.

required to ensure the structural integrity of the component [9]. This work is focused on performing thermo-fluid dynamic and mechanical analyses of the metallic M2 launcher mirror. Finally, a fatigue assessment was carried out to evaluate the number of cycles that the component can withstand, thereby estimating the operational lifetime (in cycles) in DTT.

2. Design description

2.1. Mirror design

Due to the presence of strong electromagnetic fields, two possible metallic launcher mirror configurations, characterized by lower electrical conductivity, have been considered to ensure that the resulting electromagnetic forces remain within acceptable limits for mechanical integrity:

- Launcher mirror entirely made of Inconel 718.
- Bimetallic launcher mirror with a SS316L bulk and a CuCrZr front layer.

In both design configurations, the steerable mirrors (M2) used in all DTT ECRH launchers share an identical geometry to enhance system modularity. The M2 mirror consists of an elliptical plate with a minor radius of 69 mm and a major radius of 132 mm [10]. The total thickness is set to 10 mm in both configuration (a) and (b), as shown in Fig. 2. The selected thickness is intended to provide sufficient mechanical strength under the expected operational loads. Due to the relatively low mechanical strength of Stainless Steel 316 L (SS316L), together with the high thermal loads involved, the configuration employing the monolithic material was not considered as a design hypothesis. Instead, a bimetallic design was selected to enhance thermal management by reducing and homogenizing the temperature field on the central region of the mirror, where the peak value of the ohmic load is located. In this configuration, a CuCrZr layer with variable thickness was added on the reflecting surface, with a thickness of 2 mm in the central region and 1 mm in the outer region. Furthermore, the CuCrZr layer consists of an elliptical plate with a minor radius of 34.5 mm and a major radius of 66 mm, corresponding to 50 % of the size of the mirror's ellipse itself. This idea was developed to achieve a trade-off between thermal exchange efficiency and electromagnetic forces, which are primarily influenced by the amount of CuCrZr present in the component. Additionally, at least 1 mm of SS316L was provided between the cooling water and the CuCrZr layer. This was implemented both to ensure mechanical resistance to the pressure exerted by the fluid inside the cooling system and to prevent erosion and corrosion issues that would arise from direct contact between the CuCrZr layer and water. Conversely, Inconel 718, owing to its superior mechanical performance, has been considered a viable candidate for a standalone application. Finally, both configurations will include a thin coating, on the order of a few micrometres, uniformly applied over the entire reflective surface, to ensure effective microwave reflection. The choice of coating material will be based on the thermo-mechanical compatibility with the bulk substrate, with particular attention to the coefficient of thermal expansion (CTE). A smaller mismatch in thermal expansion between the coating and the bulk material reduces interfacial stresses, thereby lowering the risk of coating delamination or failure. Among the candidate materials, copper shows the highest compatibility with the proposed bulk materials. However, this aspect will be addressed in more detail in a dedicated future publication. The present work focuses primarily on the structural design of the launcher mirror bulk.

2.2. Electromagnetic investigation

The selection of these two configurations is driven by the objective of minimizing the electromagnetic forces acting on the system, particularly during plasma disruptions when such loads become more critical. Throughout the various phases of tokamak operation, ranging from plasma initiation and current ramp-up to ramp-down, the magnetic fields undergo continuous variation [11]. These time-dependent magnetic fields induce eddy currents in adjacent conductive materials, such as metal components and structural elements. In the event of unmitigated plasma instabilities, particularly magnetohydrodynamic (MHD) disturbances, plasma temperature drops and the confinement of plasma particles is lost. This abrupt variation of plasma current, referred to as disruptions, results in significant transient magnetic field variations, which in turn generate large, induced currents in surrounding conductive structures. The interaction between these eddy currents and the magnetic fields produces Lorentz forces, exerting mechanical loads on metallic parts of the tokamak. These forces can reach critical levels during disruptive events, posing risks of mechanical failure or long-term fatigue damage to structural components [8]. Indeed, a mirror made entirely of CuCrZr would exhibit poloidal and toroidal electromagnetic forces of 560.6 N and 709.1 N respectively [11]; therefore, the option of a mirror entirely in CuCrZr was discarded. As an alternative, two configurations characterized by low electrical conductivity were thus evaluated. As a result, both launcher mirror configurations exhibit limited electromagnetic force magnitudes, leading to correspondingly low electromagnetic stresses that are not expected to compromise the mechanical integrity of the component. In Section 5, the results of the electromagnetic forces evaluated for the different launcher mirror configurations are briefly reported.

2.3. Cooling system

The variable-depth complementary spiral cooling channel (VDCS), investigated in detail in a previous work [10], has been integrated into these new launcher configurations. For the Inconel 718 mirror case, as shown in Fig. 3(a), the cooling channel has been modified near the inlet region to increase the wetted surface area, particularly in the central zone, which is the most critical in terms of thermal load, always maintaining the minimum thickness required by the component's manufacturing process. The aim was to maximize the wetted area in order to increase the effective heat exchange surface and improve thermal performance in materials with low thermal conductivity, such as Inconel. As illustrated in the zoomed view of the Fig. 3(a), the inlet was enlarged to enhance heat transfer and mitigate hotspots arising from the intrinsic thermal resistance of the material. In the case of the bimetallic configuration, shown in Fig. 3(b), the cooling channel has been extended in the outlet region instead to achieve a more uniform temperature distribution across the mirror. As will be shown in the results section, these slight modifications to the cooling channel do not lead to a significant increase in pressure drop compared to the originally designed channel, thus confirming the feasibility of the proposed changes from a fluid dynamic standpoint.

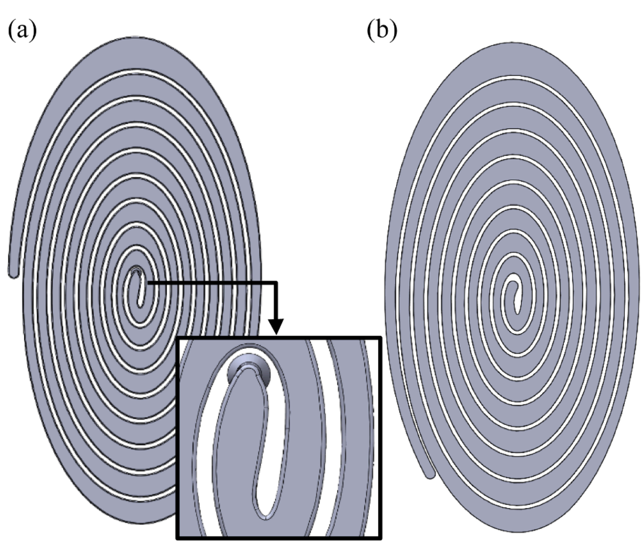

Fig. 3. (a) Cooling system tailored for the monolithic Inconel 718 configuration. (b) Cooling system tailored for the bimetallic SS316L/CuCrZr configuration.

3. Fluid-dynamic analysis

3.1. Computational model

The conjugate heat transfer problem is solved numerically under steady-state conditions using the STAR-CCM+ simulation software [12]. The analysis focuses on determining the velocity, pressure, and temperature fields within the M2 mirror. A segregated approach is employed for the fluid flow computation. Given the fully turbulent nature of the flow throughout the cooling channel, the Reynolds-Averaged Navier-Stokes (RANS) formulation is used, specifically the two-layer realizable k-ε turbulence model with y^+ adaptive wall treatment, as described in [10]. This model is capable of effectively resolving flow characteristics in both low and high y^+ regions by dynamically adjusting its near-wall modelling strategy. It is well-suited for capturing complex flow phenomena such as rotation, separation, and steep velocity or pressure gradients, offering accurate prediction of turbulence behaviour in proximity to solid boundaries.

3.2. Boundary conditions

The boundary conditions are established according to the expected operating conditions of the DTT system reported in [10]. At the coolant inlet, a constant flow rate of 10 l/min is imposed, along with a fixed temperature of 50 °C. The outlet is set to a pressure of 4 bar. Water serves as the cooling fluid, and its thermophysical properties are implemented following the IAPWS-97 formulation, ensuring precise tracking of saturation parameters [12]. The thermal characteristics of the solid materials are also defined within the model. The thermophysical properties of the solid materials, Inconel 718, SS316L, and CuCrZr, are taken from the ITER Materials Properties Handbook [13] and implemented in the computational model. Temperature-dependent variations of these properties are accounted for to ensure accurate thermal and mechanical analysis. Subsequently, the applied heat sources include microwave power absorption (P_{mw}), plasma radiation (P_{pl}), and volumetric neutron heating (P_{pl}), incorporated as described below [10]:

- $P_{mw} = A_{mw}\frac{2Q}{\pi w_x w_y} e^{-2\left(\left(\frac{x}{w_x}\right)^2 + \left(\frac{y}{w_y}\right)^2\right)}$ MW/m^2
- $P_{pl} = 0.1768$ MW/m^2
- $P_n = 10$ kW/m^3

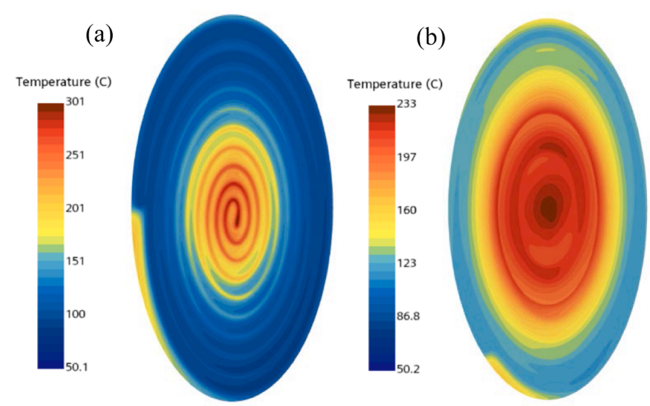

Fig. 4. (a) Mirror temperature profile for the monolithic Inconel 718 configuration. (b) Mirror temperature profile for the bimetallic SS316L/CuCrZr configuration.

With beam power $Q = 1$ MW, absorption coefficient A_{mw} depending on surface material properties, and beam radii w_x and w_y evaluated for a 58° incident angle (worst case scenario) equal to 43 mm and 81.1 mm, respectively, it results in a central peak power density of 1.874 MW /m^2 [10].

3.3. Results

This section reports the results of the CFD simulation for both launcher mirror configurations. As shown in the Fig. 4, the Inconel-only configuration, characterized by a lower thermal conductivity compared to SS316L and much lower than CuCrZr, exhibits a peak temperature of 301 °C at the cooling channel wall. In contrast, the bimetallic configuration achieves a lower peak temperature of 233 °C. Indeed, the CuCrZr layer, owing to its high thermal conductivity, enhances radial heat dissipation across the mirror surface. This results not only in a reduction of the peak temperature but also in a more uniform temperature distribution over the entire mirror. As previously discussed, the stainless steel–only option was excluded from the analysis, since the resulting thermomechanical stresses would exceed the material's intrinsic strength limits. Indeed, the average thermal conductivity of Inconel 718 is approximately 13.32 W/m·K, while that of SS316L is around 16.27 W /m·K. Given the comparable thermomechanical properties of the two materials, this leads to similar temperature and stress fields distribution. At the same time, being the yield strength of the SS316L much lower than that of the Inconel 718, the mirror would not withstand the load. On the other hand, the pressure throughout the modified cooling channel remains within the acceptable operational range defined by the DTT ECRH system. With an imposed absolute outlet pressure of 4 bar, the inlet pressure reaches 10.19 bar for the Inconel configuration and 8.93 bar for the bimetallic one. Table 1 reports the comparison of the absolute pressure drop in the modified channel designs relative to the original baseline configuration, highlighting the fluid dynamic impact of the proposed geometrical adjustments. From this comparison, the feasibility of slightly modifying the cooling channel to increase the heat exchange surface, particularly in the central region, is evident, without causing a significant rise in pressure drop. Specifically, the modified inlet region leads to a 27.37 % increase in pressure drop for the Inconel configuration compared to the original design, whereas for the SS316L/CuCrZr configuration the increase of pressure is limited to 1.44 %. Finally, despite the elevated peak temperatures observed, no boiling or cavitation phenomena occur during operation in the bimetallic mirror configurations. In the Inconel mirror configuration, however, both phenomena are present; since the constraints on the total system pressure are an outlet pressure of 4 bar and a maximum inlet pressure of 12 bar, this issue could potentially be mitigated by increasing the total system pressure by approximately 1 bar.

4. Thermo-mechanical analysis

4.1. Geometry and mesh

After optimizing the cooling channel and the CuCrZr layer thickness to enhance thermal exchange, structural analyses based on fluid-structure interaction (FSI) were performed to assess the mechanical integrity of the two metallic configurations. Prior to setting up the simulation, the mirror geometry was updated to include flexible supports, thereby providing realistic boundary conditions for the component. The right side of the Fig. 5 shows the same supports added to the mirror geometry for both the Inconel and SS316L-CuCrZr configurations [14]. For the thermo-mechanical study, the updated geometry was imported into ANSYS Mechanical [15]. Temperature-dependent thermomechanical properties of the materials were assigned to ensure an accurate structural response. Subsequently, a tetrahedral mesh was generated for both the mirror and the flexible supports. However, the primary aim of this study is to define and simulate the design of the mirror's bulk structure, therefore, the supports, after being meshed together with the geometry, are included solely to apply realistic boundary constraints. A dedicated paper will address the detailed design of the support system, including its geometry and potential candidate materials for manufacturing.

Table 1
Pressure drop along the cooling channel.

Cooling configuration	ΔP [*bar*]
VDCS [10]	4.86
Monolithic Inconel 718	6.19
Bimetallic: SS316L/CuCrZr	4.93

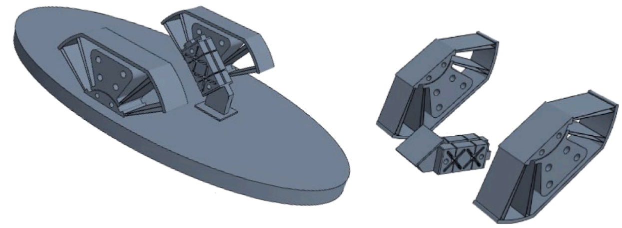

Fig. 5. Updated bulk mirror design with rear flexible supports.

4.2. Boundary conditions and loads

For the mechanical simulation, both thermal and pressure boundary conditions, as well as structural constraints on the supports, were applied. Prior to imposing these constraints, a thermal conduction analysis was performed to obtain the temperature distribution within the supports. Although the supports should be included in the overall thermofluid-dynamic analysis, this decoupled approach significantly reduced computational time: the temperature field computed from the mirror simulation was subsequently used as input for the conduction analysis on the supports. Furthermore, the expected neutron load for DTT is 10 kW/m^3; for the support setup, this corresponds to a load contribution of 0.45 W, which was therefore neglected in this analysis. The thermal results for the supports in both proposed configurations, Inconel 718 and SS316L/CuCrZr, are presented in Fig. 6. The temperature field of the mirror and the pressure distribution within the cooling channel were imported from STAR-CCM+, and the flexible supports were constrained to realistically replicate the structural boundary conditions by fixing the highlighted area, as shown in Fig. 6(c). Finally, in this study, electromagnetic stresses are not taken into account, although they would increase the resultant mechanical stresses experienced by the mirror. Since the electromagnetic analysis of the M2 mirror is still ongoing, this paper only references the estimated electromagnetic forces reported in Section 5, assuming that, due to their low magnitude, they will not significantly increase the final mechanical stresses. Indeed, the selection of these materials, as well as the choice of a specific CuCrZr layer thickness, follows the design criterion of minimizing electromagnetic forces acting on the component, thereby finding a trade-off between these forces and thermal exchange efficiency.

4.3. Results

4.3.1. Code assessment

The design validation of the M2 launcher mirror for both configurations is carried out in accordance with the design-by-analysis criteria outlined in the SDC-IC guidelines [16]. An elastic analysis method is adopted to evaluate potential plastic collapse and ratcheting effects, and to perform fatigue assessment. In this method the stresses are computed using an elastic analysis and classified into categories for their

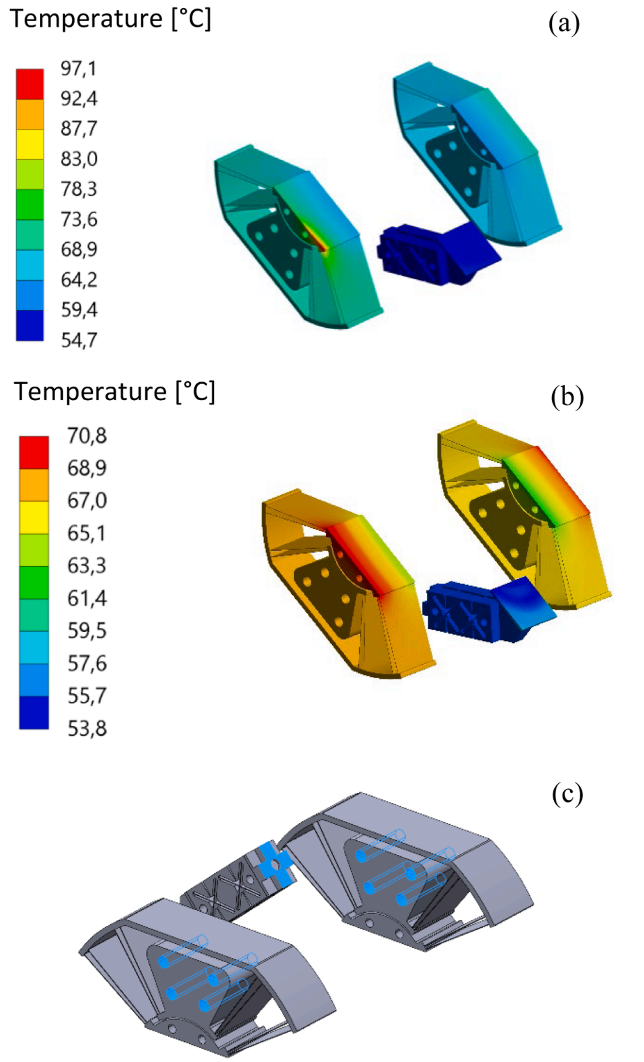

Fig. 6. (a) Supports temperature profile for the monolithic Inconel 718 configuration. (b) Supports temperature profile for the bimetallic SS316L/CuCrZr configuration. (c) Realistic boundary constraints on the supports for the FEM simulation.

comparison with the allowable limits. This stress categorization is performed by linearizing the stress (membrane, bending and peak) along the Supporting Line Segment (SLSs) [8]. These evaluation lines are defined across the regions exhibiting the highest stress levels through the material thickness, ensuring the structural integrity of the most critical zones. Furthermore, in areas with material discontinuities, such as in the bimetallic mirror configuration, a single path is traced through the composite section. In this case, the strength criterion considers a weighted allowable stress limit derived from the mechanical properties of both constituent materials. To ensure protection against ratcheting, the following criteria must be satisfied [16]:

$$\overline{P_m} \leq S_m(T_k) \tag{1}$$

$$\overline{P_L + P_b} \leq 1.5 \cdot S_m(T_k) \tag{2}$$

$$\text{Max}(\overline{P_L + P_b}) + \overline{\Delta Q} \leq 3 \cdot S_m(T_k) \tag{3}$$

Where $\overline{P_m}$ is the general primary membrane intensity, $\overline{P_L}$ is the general local membrane intensity, $\overline{P_L + P_b}$ is the primary membrane plus bending stress intensity, $\text{Max}(\overline{P_L + P_b})$ is the sum of the maximum stress value, $\overline{\Delta Q}$ is the secondary stress range value, and S_m is the allowable stress value at the corresponding temperature. In the case of composite materials, according to the SDC-IC rules, S_m accounts for all the materials present in the section. Therefore, it is calculated as follows [16]:

$$S_m^* = \frac{1}{h} \sum_{k=1}^{k=n} \left[h_k S_{m,k}(T_k) \right] \tag{4}$$

Where h is the total thickness, h_k and $S_{m,k}$ represent the thickness and the allowable stress, respectively, of the k-th material forming the composite structure.

4.3.2. *Thermo-mechanical stresses and deformation*

Fig. 7 shows the cross-sections of the two mirror configurations where stress linearization has been applied along segments traced through the corresponding thickness, while Tables 2 and 3 present the thermomechanical stress results together with the corresponding strength limits for both proposed configurations. Furthermore, the analysis of these results, obtained through the SCL, allows for the estimation of a safety factor with respect to the demanding criterion. This safety factor is defined as the ratio between $3 \cdot S_m$ and the maximum linearized stress acting on the component. For the full-Inconel configuration, this value is equal to 2.34, while the bimetallic configuration exhibits a lower safety factor of 1.30. This reduction is attributed to the inherently lower thermomechanical properties of both stainless steel and CuCrZr compared to Inconel. Nevertheless, the results confirm that both configurations fall within the operational limits, making them viable options for the construction of the launcher mirror. Finally, the deformation of the mirror under the previously described loads has been evaluated. Both configurations exhibit acceptable deformation levels that would not significantly affect the system's optical performance. As shown in Fig. 8(a), the Inconel configuration demonstrates a lower overall deformation, with a peak value of 0.58 mm located at the mirror edge. Furthermore, the Z-directional (axis perpendicular to the reflecting surface) deformation indicate that the central region experiences the least displacement. On the other hand, the bimetallic configuration, while exhibiting slightly higher deformation levels, also remains within reasonable values, as illustrated in Fig. 8(b), with a maximum of 1.25 mm. In this case as well, the Z-displacement profile shows peak deformation in the peripheral regions, while the central area remains minimally affected. In both configurations, this behaviour is due to the structure and symmetry of the supports, which keep the central area of the mirror nearly undeformed. Indeed, by analysing the induced deviation in the deformed geometries of both configurations, it was found to be negligible with respect to the plasma distance. However, a more pronounced defocusing of the reflected beam is found for the bimetallic option than the Inconel one, thus making the monolithic configuration preferable. Nevertheless, these values could be further improved by reinforcing the rear side of the mirror; future studies will investigate this aspect in greater detail. Finally, although the Inconel 718 launcher mirror exhibits higher peak temperatures, the maximum deformation is lower than that of the bimetallic launcher configuration. This behaviour can be attributed to the intrinsic thermomechanical properties of the material: Inconel 718 exhibits a higher Young's modulus than SS316L/CuCrZr and, simultaneously, a lower coefficient of thermal expansion. Consequently, these properties mitigate the deformation of the Inconel 718 launcher mirror relative to the bimetallic one.

4.4. *Fatigue evaluation*

Fatigue assessment is performed to estimate the number of cycles the component can withstand before failure, in accordance with the SDC-IC

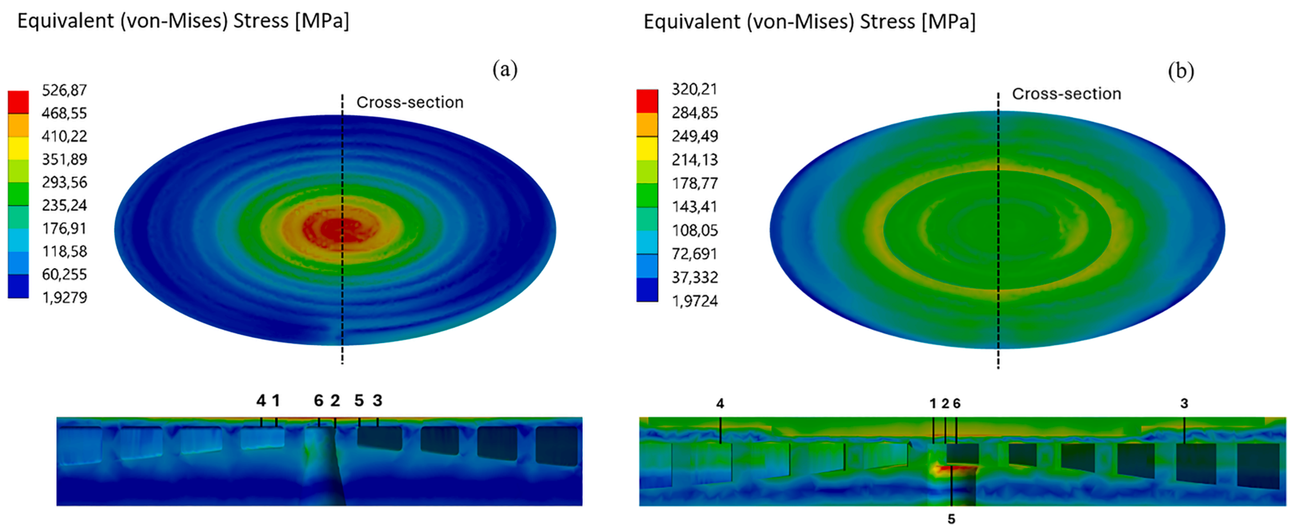

Fig. 7. Von Mises stress distribution and SLSs for the M2 mirror stress verification in both configurations: (a) Inconel 718 and (b) SS316L/CuCrZr.

Table 2
Stress verification of the M2 mirror: configuration Inconel 718, values in MPa.

SCL	1	2	3	4	5	6	Limit
$\overline{P_m}$	5.84	5.83	7.99	7.69	8.34	10.99	414
$\overline{P_L + P_b}$	23.89	39.88	27.24	26.09	44.39	31.46	621
Max$(\overline{P_L + P_b})$ + $\overline{\Delta Q}$	511.59	509.52	513.32	513.74	515.87	529.81	1242

Table 3
Stress verification of the M2 mirror: configuration SS316L/CuCrZr, values in MPa.

SCL	1	2	3	4	5	6	Limit
$\overline{P_m}$	1.82	2.35	1.96	2.58	1.67	2.61	124
$\overline{P_L + P_b}$	5.16	5.32	5.34	4.15	4.75	3.94	186
Max$(\overline{P_L + P_b})$ + $\overline{\Delta Q}$	231.46	249.15	280.65	272.78	286.75	263.04	372

code [16,17]. In the load step sequence definition, as indicated in Table 4, the temperature field is considered as the cyclic load that may lead to component failure. This study is thus conducted by calculating the stresses and/or strains on the mirror, depending on the material under consideration by the ITER Materials Properties Handbook [13]. For the Inconel 718 the difference between the stresses obtained under cyclic load (temperature load) and those under constant load (dead weight and pressure load) is as follows:

$$\Delta\sigma_{VM} = \sqrt{\frac{1}{2}\left[(\Delta\sigma_{11} - \Delta\sigma_{22})^2 + (\Delta\sigma_{22} - \Delta\sigma_{33})^2 + (\Delta\sigma_{33} - \Delta\sigma_{11})^2\right] + 3\left(\Delta\sigma_{12}^2 + \Delta\sigma_{23}^2 + \Delta\sigma_{31}^2\right)} \tag{5}$$

Each $\Delta\sigma_{ii}$ and $\Delta\sigma_{ij}$ within the Eq. (5) is obtained as the difference in normal and shear stress values between step 2 and step 3 [16]. Once the $\Delta\sigma_{VM}$ parameter is calculated, it is possible to evaluate the maximum number of cycles the structure can withstand under these thermo-mechanical stress conditions. The number of cycles is extrapolated from the table provided in the ITER Materials Properties Handbook for the Inconel 718 material [13].

For the bimetallic mirror configuration, the procedure foreseen to analyse composite material separately as if it were two independent components, ensuring that each meets the required number of cycles. If this is not the case, a conservative criterion is applied by selecting the smaller number of cycles as the allowable fatigue life for the mirror, thus ensuring the safety of the entire composite material. For this configuration, the SDC-IC guidelines prescribe fatigue analysis based on the calculation of the strain range as follows:

$$\overline{\Delta\varepsilon} = \overline{\Delta\varepsilon_1} + \overline{\Delta\varepsilon_2} + \overline{\Delta\varepsilon_3} + \overline{\Delta\varepsilon_4} \tag{6}$$

$$\overline{\Delta\varepsilon_1} = \frac{2}{3}\frac{1+\nu}{E}\overline{\Delta\sigma_{\text{tot}}} \tag{7}$$

$$\overline{\Delta\varepsilon_3} = (k_\varepsilon - 1)\left(\overline{\Delta\varepsilon_1} + \overline{\Delta\varepsilon_2}\right) \tag{8}$$

$$\overline{\Delta\varepsilon_4} = (k_\nu - 1)\,\overline{\Delta\varepsilon_1} \tag{9}$$

where $\overline{\Delta\varepsilon_1}$ is the strain given by the elastic analysis, $\overline{\Delta\varepsilon_2}$ is the plastic

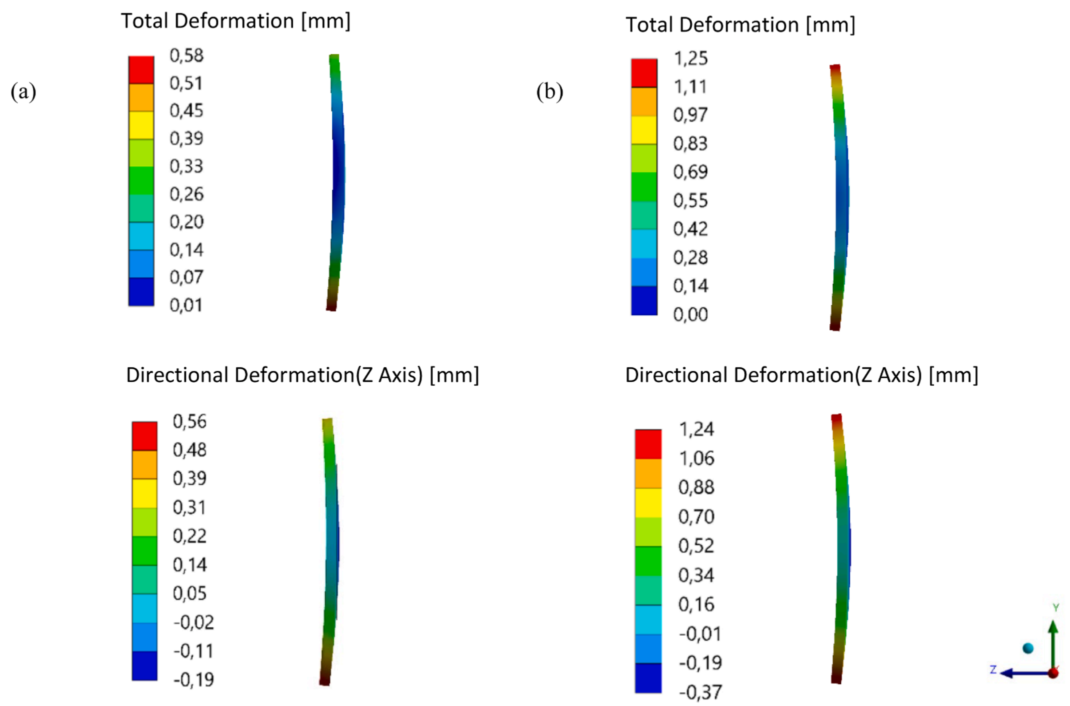

Fig. 8. Total and directional deformation (z axis) in both configurations: (a) Inconel 718 and (b) SS316L/CuCrZr.

Table 4
Load steps.

Loads	Steps		
	1	2	3
Dead weight	√	√	√
Pressure field	–	√	√
Temperature field	–	–	√

strain induced by cyclic primary stress and in this specific case this value is assumed to be 0, $\overline{\Delta\varepsilon_3}$ is the amplification of plastic strain due to elastic follow-up, and $\overline{\Delta\varepsilon_4}$ is the amplification of plastic strain due to multi-axial Poisson's effect [17].

As in the previous case, once the strain range is calculated, it is possible to determine the corresponding number of cycles from the ITER Materials Properties Handbook [13]. For the bimetallic mirror, this calculation is performed separately for both SS316L and CuCrZr to evaluate their respective fatigue lives.

Table 5 reports the calculated stress and strain values for both cases, along with the corresponding number of cycles that each component can withstand.

Finally, for the DTT machine, 25,000 pulses are expected. Therefore, considering the allowable number of cycles for each configuration, it is possible to estimate the number of thermal cycles per pulse, which amount to 8 for Inconel 718 and 4 for SS316L/CuCrZr. This parameter represents a design safety factor for the component. Both configurations are capable of withstanding at least one thermal cycle per applied pulse. A value greater than unity indicates that the component can sustain multiple thermal cycles under operational conditions.

5. Comparison among different configurations

Thermo-fluid dynamic and structural simulations were conducted on various designs to identify the optimal trade-off among hypothetical electromagnetic forces due to the material, temperature field,

Table 5
Summary of the fatigue evaluation for both configurations of the M2 mirror.

Mirror Configuration	$\Delta\sigma_{VM}$ [MPa]	$\overline{\Delta\varepsilon}$ [%]	N [Cycles]	Thermal cycles per pulse [–]
Inconel 718	262.85	-	$2 \cdot 10^5$	8
SS316L/CuCrZr	319.37/248.72	0.19/0.22	10^5	4

Table 6
Comparison of the M2 mirror configurations in terms of peak temperature, maximum deformation and stress, allowable stress limit (according to the code assessment [16]) with corresponding safety factor, fatigue life (number of cycles, again according to the code assessment [16]), and evaluation of poloidal and toroidal electromagnetic forces [11].

Mirror Configuration	Temp [°C]	Def [mm]	Max Stress [MPa]	Limit [MPa]	Safey factor [-]	N of cycles [-]	F_{pol}[N]	F_{tor}[N]
Inconel 718	300	0.57	530	1242	2.3	$2 \cdot 10^5$	10.3	12.8
Inconel 718/CuCrZr	260	0.97	460	771	1.7	10^3	27.5	34.3
SS316L/CuCrZr (a)	234	0.96	340	351	1.03	10^4	34	42.4
SS316L/CuCrZr (b)	235	0.98	343	351	1.02	10^4	26.3	32.8
SS316L/CuCrZr (c)	229	1.1	234	330	1.4	$\approx 10^5$	52.3	65.1
SS316L/CuCrZr (d)	233	1.24	287	372	1.3	10^5	30.6	38.2

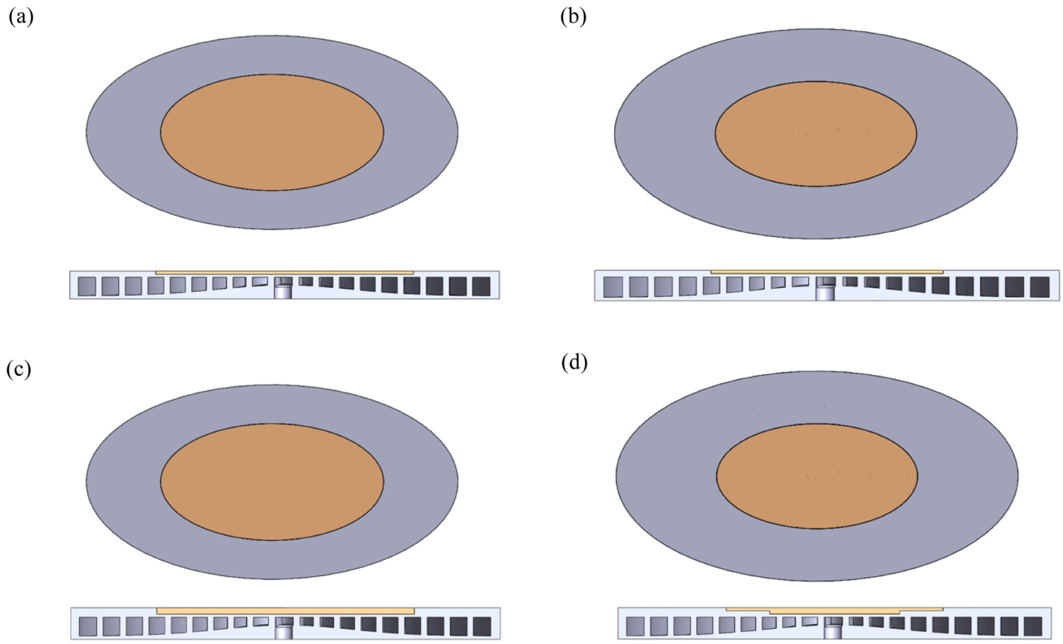

Fig. 9. Multiple configurations of the SS316L bimetallic mirror in combination with different CuCrZr layer thicknesses.

thermomechanical stresses, and fatigue life. A potential bimetallic configuration composed of Inconel and CuCrZr was also investigated. Table 6 summarizes the different cases analysed with configurations of Inconel and SS316L/CuCrZr. As shown, the bimetallic Inconel 718/CuCrZr configuration was discarded because the fatigue life it could sustain is very low, mainly due to the different mechanical properties of CuCrZr with respect to the Inconel 718. As shown in Fig. 9, for the SS316L/CuCrZr configurations, four different designs, based on the size of the CuCrZr layer, are investigated. Increasing this portion enhances thermal exchange and reduces the temperature of the mirror, but it also leads to higher electromagnetic forces [9]. Therefore, the goal was to find a trade-off between these values:

- Configuration (a) features a CuCrZr layer sized at 60 % of the actual dimensions of the elliptical face of the mirror, with a thickness of 1 mm.
- Configuration (b) features a CuCrZr layer sized at 50 % of the actual dimensions of the elliptical face of the mirror, with a thickness of 1 mm.
- Configuration (c) features a CuCrZr layer sized at 60 % of the actual dimensions of the elliptical face of the mirror, with a thickness of 2 mm.
- Configuration (d), the current final one, features a transition in the CuCrZr layer, with a thickness varying from 2 mm to 1 mm over 30 % to 50 % of the actual dimensions of the elliptical face of the mirror. This approach enhances thermal exchange while limiting the CuCrZr content, which would otherwise increase the electromagnetic forces acting on the component.

From this comparison, it is evident that increasing the thickness of the CuCrZr layer (case c) enhances radial thermal exchange and consequently reduces thermomechanical stresses, albeit with an increase in electromagnetic forces. Although this configuration provides the best safety factor, configuration (d) was preferred due to a slight increase in thermomechanical stresses but significantly more acceptable electromagnetic force levels. Indeed, this paper focuses solely on the thermomechanical analysis of the mirror, without including the electromagnetic forces. However, these forces, preliminary estimated with the procedure described in [11] are used as a criterion to evaluate the best trade-off and, consequently, the optimal design for the launch mirror. In subsequent papers, the comprehensive thermomechanical results, accounting for both thermomechanical and electromagnetic stresses, will be presented. Moreover, all configurations include a 1 mm SS316L layer between the cooling channel and the CuCrZr layer. This 1 mm thickness is an intrinsic limit to ensure both the structural robustness of the component against the pressure exerted by the coolant inside the channel and to prevent erosion and corrosion caused by direct contact between water and the CuCrZr layer. Finally, from a fatigue life perspective as well, configuration (d) outperforms configuration (c), due to the reduced amount of CuCrZr, which has inferior mechanical properties compared to SS316L, thereby lowering the fatigue life. The corresponding number of cycles is again calculated following the code assessment [16], based on the evaluated stresses and strains.

6. Conclusion

This paper presents an overview of the potential implementation of a metallic material for the DTT ECRH steering mirror. The study focuses primarily on two configurations: a monolithic Inconel 718 design and a bimetallic configuration comprising SS316L with a CuCrZr layer. The choice of the bimetallic design is motivated by the limited mechanical strength and poor thermal conductivity of monolithic SS316L under the component's thermal load conditions.

The cooling system, originally designed and detailed in previous studies [10], was adapted for these two configurations, once again confirming the thermal exchange efficiency provided by the internal channel geometry. Subsequently, based on the thermo-fluid dynamic results, both mechanical and fatigue analyses were conducted in accordance with the guidelines of the SDC-IC code [16] and the material properties specified in the ITER handbook [13]. This comprehensive study demonstrates that both proposed configurations exhibit mechanical stress values well below the material strength limits, as well as sufficiently high fatigue life compatible with the operational requirements of the DTT machine. However, due to the material properties, the thermomechanical performance of the Inconel mirror is superior to that of SS316L/CuCrZr, making it the primary candidate. Studies on manufacturing feasibility are still ongoing and will ultimately determine the material choice for the future ECRH mirror of DTT.

Finally, a comparison was conducted among different launcher mirror configurations, including monolithic materials (Inconel 718) and various bulk material combinations (SS316L and Inconel 718) with CuCrZr layers. This comparison aims to highlight the importance of achieving a trade-off between improved thermal exchange and the poloidal and toroidal electromagnetic forces acting on the component.

CRediT authorship contribution statement

Alfredo Pagliaro: Conceptualization. **Avelino Mas Sánchez:** Supervision. **Francesco Braghin:** Supervision. **Alessandro Bruschi:** Supervision. **Daniele Busi:** Supervision. **Francesco Fanale:** Supervision. **Gustavo Granucci:** Supervision. **Cinta Marraco Borderas:** Supervision. **Afra Romano:** Supervision. **Anastasia Xydou:** Supervision. **Fabio Zanon:** Supervision.

Declaration of competing interest

The authors declare that they have no known competing financial interests or personal relationships that could have appeared to influence the work reported in this paper.

Acknowledgements

The work was carried out in the framework of a PhD co-funded by Eni S.p.A. in the framework of the Italian PNRR (Piano Nazionale di Ripresa e Resilienza) in cooperation of the DTT project. The authors wish to thank all colleagues involved in the project for their precious contributions to its completion, in particular the research group from the Swiss Plasma Center (SPC) at EPFL.

Data availability

The data that has been used is confidential.

References

[1] F. Romanelli, et al., Divertor Tokamak Test facility project: status of design and implementation, Nucl. Fusion 64 (2024), https://doi.org/10.1088/1741-4326/ad5740.
[2] G. Granucci, et al., Roles of ECH system in DTT plasma operations, Nucl. Fusion 64 (2024), https://doi.org/10.1088/1741-4326/ad7742.
[3] S. Garavaglia, et al., Progress of DTT ECRH system design, Fusion Eng. Des. 168 (2021) 112678, https://doi.org/10.1016/J.FUSENGDES.2021.112678. Art. no.
[4] A. Moro, et al., Progress and challenges of the ECH transmission line design for DTT, Fusion Eng. Des. 202 (2024), https://doi.org/10.1016/J.FUSENGDES.2024.114391.
[5] F. Fanale, et al., Status of DTT ECH Transmission lines and Antennae, IEEE Trans. Plasma Sci. (2024), https://doi.org/10.1109/TPS.2024.3382745.
[6] D. Busi, et al., In-vessel piezoelectric actuation system for DTT ECRH launchers: conceptual design, Fusion Eng. Des. 180 (2022) 113196, https://doi.org/10.1016/J.FUSENGDES.2022.113196. Art. no.
[7] E. Gajetti, et al., A new efficient mirror cooling for the transmission line of fusion reactor ECH systems based on triply periodic minimal surfaces, IEEE Trans. Plasma Sci. (2024), https://doi.org/10.1109/TPS.2024.3383275.
[8] A.Mas Sanchez, et al., Fluid-dynamic and thermo-mechanical analyses of the ITER electron cyclotron Miter bend mirror for the off-centered beam scenario, Fusion Eng. Des. 192 (2023) 113643, https://doi.org/10.1016/J.FUSENGDES.2023.113643. Art. no.
[9] A. Bruschi, et al., Challenges of the DTT ECH Launchers and Options Under Study, IEEE-Transactions on Plasma Science, 2023 submitted to.
[10] A. Pagliaro, et al., Variable-depth complementary spiral cooling channel design for the steerable ECRH mirrors of DTT, Fusion Eng. Des. 219 (2025) 115276, https://doi.org/10.1016/j.fusengdes.2025.115276. Art. no.
[11] D. Busi, et al., Study of magnetic effects on DTT ECRH front-steering mirror, Fusion Eng. Des. 191 (2023) 113550, https://doi.org/10.1016/J.FUSENGDES.2023.113550. Art. no.
[12] Siemens CD-adapco. *STAR-CCM+ user guide.* 2020.
[13] ITER, Material Properties Handbook, ITER_D_222RLN, 2013.
[14] D. Busi, et al., Elastic Force Compensation Via Negative Stiffness Mechanism For the ECRH Steering Launcher of DTT, IEEE-Transactions on Plasma Science, 2013 submitted to.
[15] "ANSYS, Engineering Simulation Software, 2013", http://www.ansys.com/.
[16] In-vessel Components, Sdc-Ic_222rhc, 2012.
[17] M. Vagnoni, et al., Design optimization of the Upper Steering Mirror Assembly (USMA) for ITER ECHUL in view of disruptive events, Fusion Eng. Des. 167 (112343) (2021), https://doi.org/10.1016/j.fusengdes.2021.112343. Art. no.